Non-Hermitian Symmetry Orthogonal Frequency Division Multiplexing for Multiple-Input Multiple-Output Visible Light Communications

Chen Chen, Wen-De Zhong, and Dehao Wu

***Abstract*—Multiple-input multiple-output (MIMO) is a natural and effective way to increase the capacity of white light-emitting diode (LED) based visible light communication (VLC) systems. Orthogonal frequency division multiplexing (OFDM) using high-order modulation is another widely used technique in VLC systems. Due to the intensity modulation and direct detection nature of VLC systems, Hermitian symmetry is usually imposed in OFDM so as to obtain a real-valued signal. In this paper, we investigate a non-Hermitian symmetry OFDM (NHS-OFDM) scheme for MIMO-VLC systems. By transmitting the real and imaginary parts of a complex-valued OFDM signal via a pair of white LEDs, NHS-OFDM circumvents the constraint of Hermitian symmetry. We evaluate the performance of an indoor 2×2 MIMO-VLC system using conventional Hermitian symmetry-based OFDM (HS-OFDM) and NHS-OFDM, where both a non-imaging receiver and an imaging receiver are considered. Analytical results show that the system using NHS-OFDM achieves superior bit error rate (BER) performance to that using HS-OFDM, with lower or nearly the same computational complexity. The superior BER performance of NHS-OFDM-based MIMO-VLC is further verified by experiments. The experimental results demonstrate that, in a 400 Mb/s 2×2 MIMO-VLC system with an imaging receiver, NHS-OFDM improves the communication coverage by about 30% compared with conventional HS-OFDM for a target BER of 3.8×10^{-3}.**

***Index Terms*—Multiple-input multiple-output (MIMO); Orthogonal frequency division multiplexing (OFDM); Visible light communication (VLC).**

I. Introduction

White light-emitting diode (LED) enabled visible light communication (VLC) has attracted great interest in recent years because it can provide simultaneous illumination and high-speed wireless access in indoor environments [1–3]. Even though VLC exhibits many exciting advantages such as potentially large license-free bandwidth, high security, and electromagnetic interference-free operation, there are still several technical challenges that hinder the development of high-speed VLC systems. Specifically, the overall capacity of VLC systems is limited by the small modulation bandwidth of LEDs [4]. So far, many techniques have been proposed to increase the capacity of VLC systems, including analog and digital equalization [5,6], multiple-input multiple-output (MIMO) transmission [7–9], orthogonal frequency division multiplexing (OFDM) using high-order modulation [10,11], and adaptive modulation [12]. Some of these techniques can be combined together to further improve the system capacity. For example, an OFDM-based MIMO scheme with both pre- and post-equalization was reported to achieve 1.1 Gb/s VLC transmission [13].

Because the light emitted by LEDs is naturally incoherent, intensity modulation/direct detection (IM/DD) is generally used, and only real-valued signals can be transmitted in VLC systems [10]. To obtain LED-compatible unipolar real-valued OFDM signals, Hermitian symmetry (HS) is usually imposed before performing the inverse fast Fourier transform (IFFT) and is followed by adding a DC bias [10–13]. HS-based OFDM (HS-OFDM) with a DC bias is also known as DC-biased optical OFDM (DCO-OFDM) [14]. Many modified HS-OFDM schemes have been reported in the literature for spectral efficiency improvement and/or peak-to-average power ratio reduction, such as asymmetrically clipped optical OFDM (ACO-OFDM) [14], unipolar OFDM (U-OFDM) [15], enhanced U-OFDM (eU-OFDM) [16], spectral and energy efficient OFDM (SEE-OFDM) [17], and asymmetrically and symmetrically clipped optical OFDM (ASCO-OFDM) [18]. However, imposing HS doubles the sizes of IFFT and FFT. In recent years, a few approaches have been proposed to circumvent the HS constraint of OFDM for IM/DD optical systems. A real-valued OFDM scheme based on fast Hartley transform (FHT) was reported in [19], where the Fourier processing was replaced by the real processing of the Hartley transform; however, only real constellations can be used. Based on a polar representation of complex symbols, polar OFDM (P-OFDM) was proposed, which can offer a doubled spectral efficiency as ACO-OFDM [20,21]. Moreover, the idea of extracting the real (Re) and imaginary (Im) parts of a complex-valued OFDM signal and separately transmitting them via multiple consecutive symbols was reported in [22,23]. However, using multiple symbols to

Manuscript received March 24, 2016; revised July 23, 2016; accepted November 4, 2016; published December 16, 2016 (Doc. ID 261854).

The authors are with the School of Electrical and Electronic Engineering, Nanyang Technological University, 50 Nanyang Avenue, Singapore 639798, Singapore (e-mail: chen0884@e.ntu.edu.sg).

https://doi.org/10.1364/JOCN.9.000036

transmit one OFDM frame greatly reduces the capacity. In [24,25], the Re and Im parts were separately transmitted through two chips of a RGB-LED. Because RGB-LEDs are much more expensive than phosphor-based LEDs, the use of RGB-LEDs would increase the cost of VLC systems.

In practical indoor environments, multiple white LEDs are commonly mounted in the ceiling to provide sufficient illumination. Hence, MIMO is a natural and effective way to increase the capacity of VLC systems. Two types of receivers can be used in MIMO-VLC systems, including non-imaging receivers (NImRs) and imaging receivers (ImRs) [26]. Because an ImR can demultiplex the transmitted signals and thus eliminate the inter-channel interference (ICI), ImR-based MIMO-VLC systems can achieve high spatial diversity. Due to the negligible ICI, an ImR-based MIMO is also referred to as space division multiplexing (SDM) [27–29].

Recently, we proposed a non-HS OFDM (NHS-OFDM) scheme together with a modified ImR to improve the communication coverage of indoor MIMO-VLC systems. The preliminary results have been reported in [29]. However, the principle of the proposed NHS-OFDM has not been described in detail, and the performance of MIMO-VLC systems using NHS-OFDM has not been experimentally verified. In this paper, we present an in-depth investigation of NHS-OFDM for MIMO-VLC systems where both NImR and ImR are considered. By pairwise transmitting the Re and Im parts of a complex-valued OFDM signal via two LEDs, NHS-OFDM circumvents the constraint of HS. The performance of a 2×2 MIMO-VLC system using NHS-OFDM is investigated and compared with the system using conventional HS-OFDM. Analytical and experimental results show that the system using NHS-OFDM achieves superior bit error rate (BER) performance than that using HS-OFDM. We also show that the MIMO-VLC system using NHS-OFDM has lower or nearly the same computational complexity as the system using conventional HS-OFDM. To the best of our knowledge, it is the first experimental demonstration of an indoor 2×2 MIMO-VLC system using NHS-OFDM.

The rest of the paper is organized as follows. Section II describes the model of MIMO-VLC systems using HS-OFDM and NHS-OFDM, where both NImR and ImR are considered. In Section III, we numerically analyze and compare the performance of a 2×2 MIMO-VLC system using HS-OFDM and NHS-OFDM. The experimental results are presented in Section IV. Finally, Section V concludes the paper.

II. MIMO-VLC Using HS-OFDM and NHS-OFDM

In this section, we introduce the model of MIMO-VLC systems using conventional HS-OFDM and NHS-OFDM. For simplicity and without loss of generality, a 2×2 MIMO-VLC system is considered.

A. System Model

Figures 1(a) and 1(b) illustrate the block diagrams of an indoor 2×2 MIMO-VLC system using HS-OFDM and NHS-OFDM, respectively. As shown in Fig. 1(a), two pairs of HS-OFDM transmitters and receivers are needed. The

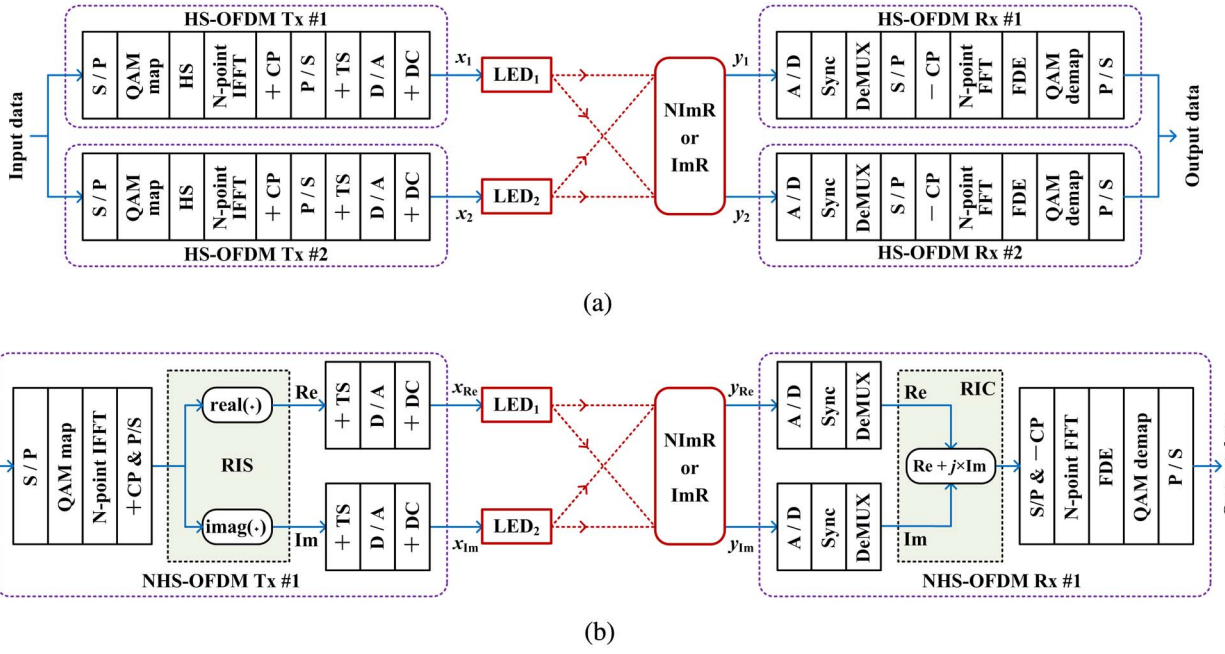

Fig. 1. Block diagrams of a 2×2 MIMO-VLC system using (a) conventional HS-OFDM and (b) NHS-OFDM. (Tx, transmitter; Rx, receiver; HS, Hermitian symmetry; NImR, non-imaging receiver; ImR, imaging receiver; RIS, real-and-imaginary separator; RIC, real-and-imaginary combiner; sync, synchronization; DeMUX, demultiplexing.)

serial input data are first split into two parallel data streams, and each stream is fed into a HS-OFDM transmitter. After serial-to-parallel (S/P) conversion, the parallel data are mapped to quadrature amplitude modulation (QAM) symbols. In order to generate a real-valued signal, HS is imposed before the N-point IFFT. A cyclic prefix (CP) is added, and the resultant parallel signal is parallel-to-serial (P/S) converted. Then, a training sequence (TS) is added. After digital-to-analog (D/A) conversion, a DC bias is added. Therefore, two unipolar analog signals $x_1(t)$ and $x_2(t)$ can be obtained at the outputs of two HS-OFDM transmitters, which are then separately modulated onto the intensities of two LEDs. After being transmitted over the free-space channel, the light is detected by a receiver, which can be a NImR or an ImR. Two output signals $y_1(t)$ and $y_2(t)$ are obtained and separately demodulated in two HS-OFDM receivers. In each HS-OFDM receiver, the received analog signal is analog-to-digital (A/D) converted. By exploiting the TS, time synchronization is performed. Based on the pre-estimated channel matrix, MIMO demultiplexing (DeMUX) is executed. After performing S/P conversion, CP removal, N-point FFT, frequency domain equalization (FDE), QAM de-mapping, and P/S conversion, an output data stream is generated. The final output data are obtained by combining the two parallel output data streams together.

As can be seen in Fig. 1(b), only one pair of the NHS-OFDM transmitter and receiver is needed in the 2×2 MIMO-VLC system using NHS-OFDM. In the NHS-OFDM transmitter, no HS is imposed before the IFFT, and a real-and-imaginary separator (RIS) is used to separate the Re and Im parts of the complex-valued OFDM signal. The intensities of two LEDs are then modulated by the Re and Im signals $x_{\mathrm{Re}}(t)$ and $x_{\mathrm{Im}}(t)$, respectively. Because transmission distances of the Re and Im signals might be different, the received Re and Im signals $y_{\mathrm{Re}}(t)$ and $y_{\mathrm{Im}}(t)$ might have different phases and different electrical powers. In order to eliminate phase imbalance, the received Re and Im signals are separately synchronized by using the corresponding TSs after A/D conversion. Moreover, the electrical powers of the received Re and Im signals are also balanced, and the power balancing can be easily achieved via usual MIMO DeMUX. The phase and power balanced Re and Im signals are combined together in a real-and-imaginary combiner (RIC) to reconstruct the complex-valued signal. It should be noted that the same synchronization and MIMO DeMUX procedures are required in HS-OFDM-based MIMO-VLC systems. Therefore, the operations for removing phase and power imbalances do not add any additional requirements in NHS-OFDM-based MIMO-VLC systems.

It is noteworthy that the proposed NHS-OFDM scheme can only be used in MIMO-VLC systems with one or more pairs of LEDs, whereas HS-OFDM can be used in both single-input single-output VLC (SISO-VLC) and MIMO-VLC systems. It can be seen that HS-OFDM, which is also known as DCO-OFDM [14], exploits HS to generate a real-valued signal and the DC bias is added. Because DC bias is also required in NHS-OFDM, NHS-OFDM can be considered as a modified DCO-OFDM scheme for MIMO-VLC, which removes the constraint of HS.

Generally, two different types of receivers can be used in MIMO-VLC systems. Figures 2(a) and 2(b) show diagrams of a 2×2 MIMO-VLC system employing a NImR and an ImR, respectively. For the 2×2 MIMO-VLC system employing a NImR, the channel matrix is given by

$$\mathbf{H}_{\mathrm{NImR}} = \begin{bmatrix} h_{11} & h_{12} \\ h_{21} & h_{22} \end{bmatrix}, \tag{1}$$

where $h_{rt}(t, r = 1, 2)$ is the optical channel gain between the tth LED and the rth PD. However, when an ImR is employed, the ICI can be substantially eliminated [28]; hence the channel matrix becomes a diagonal matrix:

$$\mathbf{H}_{\mathrm{ImR}} = \begin{bmatrix} 0 & h_{12} \\ h_{21} & 0 \end{bmatrix}. \tag{2}$$

In a typical room environment where multiple LEDs are mounted in the ceiling, a PD can detect both the line-of-sight (LOS) and diffuse components. It has been shown that light intensity of the LOS component is much higher than that of the strongest diffuse component in a typical room, so it is reasonable to only consider the LOS component in the MIMO-VLC system [7]. The LOS irradiance of an LED can be modeled as a generalized Lambertian radiation pattern, and the LOS optical channel gain is given by [29,30]

$$h_{rt} = \frac{(m+1)A}{2\pi d_{rt}^2} \mu \eta \cos^m(\varphi_{rt}) \cos(\phi_{rt}), \tag{3}$$

where $m = -\ln 2 / \ln(\cos \Psi_{1/2})$ is the order of Lambertian emission, and $\Psi_{1/2}$ is the semi-angle at half power of LED, A is the active area of PD, d_{rt} is the distance between the tth LED and the rth PD, μ and η are the gains of the optical filter and lens, respectively, φ_{rt} is the angle of irradiance, and ϕ_{rt} is the angle of incidence. It should be noted that the optical gain becomes zero if ϕ is outside the field of view (FOV) of the receiver.

Moreover, the wavelength used in VLC systems is around 380 to 750 nm, which is much smaller than the typical area of a PD; hence multipath fading can be neglected due to high spatial diversity [1,31]. Nevertheless, performance degradation is possible in the presence of multipath-induced inter-symbol interference (ISI) [2].

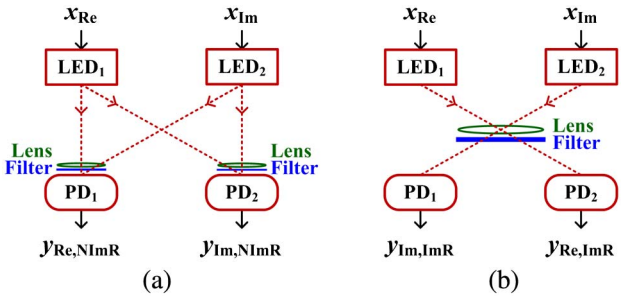

Fig. 2. Diagrams of a NHS-OFDM-based 2×2 MIMO-VLC system employing (a) NImR and (b) ImR.

B. BER Analysis

1) BER for HS-OFDM: As shown in Fig. 1(a), assuming that two LEDs have the same output optical power P_{LED} and the same modulation index ξ, and two PDs have the same responsivity R, the received signal vector $\mathbf{y} = [y_1 \quad y_2]^T$ in the 2×2 MIMO-VLC system using HS-OFDM is represented by [29]

$$\mathbf{y} = RP_{\mathrm{LED}}\xi\mathbf{H}\mathbf{x} + \mathbf{n}, \tag{4}$$

where $\mathbf{x} = [x_1 \quad x_2]^T$ is the transmitted signal vector, $\mathbf{H}$ is the channel matrix, and $\mathbf{n} = [n_1 \quad n_2]^T$ is the additive noise vector. $\mathbf{H}$ is given by Eq. (1) when a NImR is used and $\mathbf{H}$ becomes Eq. (2) when an ImR is used. $n_1(t)$ and $n_2(t)$ can be modeled as real-valued additive white Gaussian noises (AWGNs), each consisting of both shot and thermal noises [30].

In order to recover data from the received signal, MIMO DeMUX is required. So far, a lot of techniques have been proposed, of which zero-forcing (ZF) using basic channel inversion is adopted here due to its low complexity [32].

After ZF-based MIMO DeMUX and normalization, we have

$$\tilde{\mathbf{x}} = \frac{1}{RP_{\mathrm{LED}}\xi}\mathbf{H}^{-1}\mathbf{y} = \mathbf{x} + \frac{1}{RP_{\mathrm{LED}}\xi}\mathbf{H}^{-1}\mathbf{n}. \tag{5}$$

As per Eq. (5), the signal-to-noise ratios (SNRs) of two received HS-OFDM signals using a NImR are, respectively, given by

$$\begin{cases} \mathrm{SNR}_{\mathrm{HS1}}^{\mathrm{NImR}} = (RP_{\mathrm{LED}}\xi)^2 \dfrac{(h_{11}h_{22} - h_{12}h_{21})^2}{h_{22}^2\sigma_{n_1}^2 + h_{12}^2\sigma_{n_2}^2} \\ \mathrm{SNR}_{\mathrm{HS2}}^{\mathrm{NImR}} = (RP_{\mathrm{LED}}\xi)^2 \dfrac{(h_{11}h_{22} - h_{12}h_{21})^2}{h_{21}^2\sigma_{n_1}^2 + h_{11}^2\sigma_{n_2}^2} \end{cases}, \tag{6}$$

where $\sigma_{n_1}^2$ and $\sigma_{n_2}^2$ are the variances of $n_1(t)$ and $n_2(t)$, respectively. However, when an ImR is employed, h_{11} and h_{22} become zero, and hence the SNRs are given by

$$\begin{cases} \mathrm{SNR}_{\mathrm{HS1}}^{\mathrm{ImR}} = (RP_{\mathrm{LED}}\xi)^2 \dfrac{h_{21}^2}{\sigma_{n_2}^2} \\ \mathrm{SNR}_{\mathrm{HS2}}^{\mathrm{ImR}} = (RP_{\mathrm{LED}}\xi)^2 \dfrac{h_{12}^2}{\sigma_{n_1}^2} \end{cases}. \tag{7}$$

The BER of an OFDM signal using $I\times J$ rectangular QAM mapping over an AWGN channel is approximated by [33]

$$\mathrm{BER} = \frac{2}{\log_2(I\times J)}\left(\frac{I-1}{I} + \frac{J-1}{J}\right)Q\left(\sqrt{\frac{6\times\mathrm{SNR}}{I^2+J^2-2}}\right), \tag{8}$$

where $Q(\cdot)$ is the Q-function. Therefore, the BERs of the two HS-OFDM signals ($\mathrm{BER}_{\mathrm{HS1}}$ and $\mathrm{BER}_{\mathrm{HS2}}$) employing a NImR and an ImR can be obtained by substituting Eqs. (6) and (7) into Eq. (8), respectively. The average BER of the 2×2 MIMO-VLC system using HS-OFDM is given by

$$\mathrm{BER}_{\mathrm{HS}} = \frac{\mathrm{BER}_{\mathrm{HS1}} + \mathrm{BER}_{\mathrm{HS2}}}{2}. \tag{9}$$

2) BER for NHS-OFDM: When NHS-OFDM is used in the 2×2 MIMO-VLC system, as shown in Fig. 1(b), the transmitted signal vector is given by $\mathbf{x}' = [x_{\mathrm{Re}} \quad x_{\mathrm{Im}}]^T$, which corresponds to a complex-valued NHS-OFDM signal $x_{\mathrm{NHS}}(t) = x_{\mathrm{Re}}(t) + j\times x_{\mathrm{Im}}(t)$. After being transmitted over the free-space channel, the received signal vector $\mathbf{x}' = [y_{\mathrm{Re}} \quad y_{\mathrm{Im}}]^T$ is expressed by

$$\mathbf{y}' = RP_{\mathrm{LED}}\xi\mathbf{H}\mathbf{x}' + \mathbf{n}', \tag{10}$$

where $\mathbf{n}' = [n_{\mathrm{Re}} \quad n_{\mathrm{Im}}]^T$ is the additive noise vector. Similarly, ZF-based MIMO DeMUX is performed, and hence the estimated signal $\tilde{\mathbf{x}}' = [\tilde{x}_{\mathrm{Re}} \quad \tilde{x}_{\mathrm{Im}}]^T$ is obtained by

$$\tilde{\mathbf{x}}' = \frac{1}{RP_{\mathrm{LED}}\xi}\mathbf{H}^{-1}\mathbf{x}' = \mathbf{x}' + \frac{1}{RP_{\mathrm{LED}}\xi}\mathbf{H}^{-1}\mathbf{x}'. \tag{11}$$

The powers of the Re and Im parts are balanced after MIMO DeMUX, and the complex-valued NHS-OFDM signal can be reconstructed by combining $\tilde{x}_{\mathrm{Re}}$ and $\tilde{x}_{\mathrm{Im}}$ together:

$$\tilde{x}_{\mathrm{NHS}}(t) = \tilde{x}_{\mathrm{Re}} + j\times\tilde{x}_{\mathrm{Im}}(t). \tag{12}$$

As per Eq. (12), the SNR of the received NHS-OFDM signal using a NImR is given by

$$\mathrm{SNR}_{\mathrm{NHS}}^{\mathrm{NImR}} = (RP_{\mathrm{LED}}\xi)^2 \frac{2(h_{11}h_{22} - h_{12}h_{21})^2}{(h_{21}^2+h_{22}^2)\sigma_{n_{\mathrm{Re}}}^2 + (h_{11}^2+h_{12}^2)\sigma_{n_{\mathrm{Im}}}^2}, \tag{13}$$

where $\sigma_{n_{\mathrm{Re}}}^2$ and $\sigma_{n_{\mathrm{Im}}}^2$ are the variances of $n_{\mathrm{Re}}(t)$ and $n_{\mathrm{Im}}(t)$, respectively. When an ImR is employed, the SNR becomes

$$\mathrm{SNR}_{\mathrm{NHS}}^{\mathrm{ImR}} = (RP_{\mathrm{LED}}\xi)^2 \frac{2(h_{12}h_{21})^2}{h_{21}^2\sigma_{n_{\mathrm{Re}}}^2 + h_{12}^2\sigma_{n_{\mathrm{Im}}}^2}. \tag{14}$$

Substituting Eqs. (13) and (14) into Eq. (8) yields the BER of the NHS-OFDM-based 2×2 MIMO-VLC system employing a NImR and an ImR, respectively.

III. Performance Evaluation and Comparisons

In this section, we numerically evaluate the performance of a 2×2 MIMO-VLC system using conventional HS-OFDM and NHS-OFDM, based on the formulas derived in Subsection II.B. It should be pointed out that the obtained analytical results are applicable to general MIMO-VLC systems using multiple pairs of LEDs. Table I lists the key parameters of the system setup. In this analysis, we consider a 2×2 MIMO-VLC system in a 2 m × 2 m × 2.5 m room where two LEDs are mounted in the ceiling and the height of the desktop is 0.5 m. The semi-angle at half power of the LED is 60°, and the modulation index is 0.3. The gains of the optical filter and the lens are both 1. The responsivity of the PD is 1 A/W.

TABLE I
KEY PARAMETERS OF SYSTEM SETUP

Parameter	Value
Room dimension (length × width × height)	2 m × 2 m × 2.5 m
Locations of two LEDs	(−0.5, 0, 2.5) (0.5, 0, 2.5)
Height of desktop	0.5 m
Semi-angle at half power of LED	60°
Modulation index	0.3
Gain of optical filter	1
Gain of optical lens	1
Responsivity of PD	1 A/W

A. BER Performance

We first show that the system using NHS-OFDM achieves superior BER performance than the system using HS-OFDM. The SNR performance along the X direction with $Y = 0$ m is shown in Fig. 3(a), where an ImR is assumed. As we can see, the SNR values are the same for HS-OFDM and NHS-OFDM if and only if $X = 0$ m, i.e., the ImR is located at the center of the receiving plane. When the ImR is moved away from the center, the SNRs of two HS-OFDM signals become different. For example, the SNRs of two HS-OFDM signals at $X = 0.5$ m are 15.84 and 19.75 dB, respectively, whereas the SNR of the NHS-OFDM signal is 17.37 dB. It can also be observed that the SNR of the NHS-OFDM signal is always in between the SNRs of the two HS-OFDM signals. Figure 3(b) plots the relationship between BER and SNR for a 4 × 4 rectangular QAM (16QAM) based OFDM signal over an AWGN channel. The BERs of two HS-OFDM signals at $X = 0.5$ m are 2.1×10^{-3} and 5.2×10^{-6}, respectively, and the average BER of the 2 × 2 MIMO-VLC system using HS-OFDM is 1.1×10^{-3}. In contrast, the BER of the system using NHS-OFDM at $X = 0.5$ m is 3.6×10^{-4}, resulting in a significant BER reduction. Figures 3(a) and 3(b) can explain why the 2 × 2 MIMO-VLC system using NHS-OFDM has better BER performance than the system using HS-OFDM.

Figures 4(a) and 4(b) show BER versus receiver position offset along the X direction with $Y = 0$ m for the 2 × 2

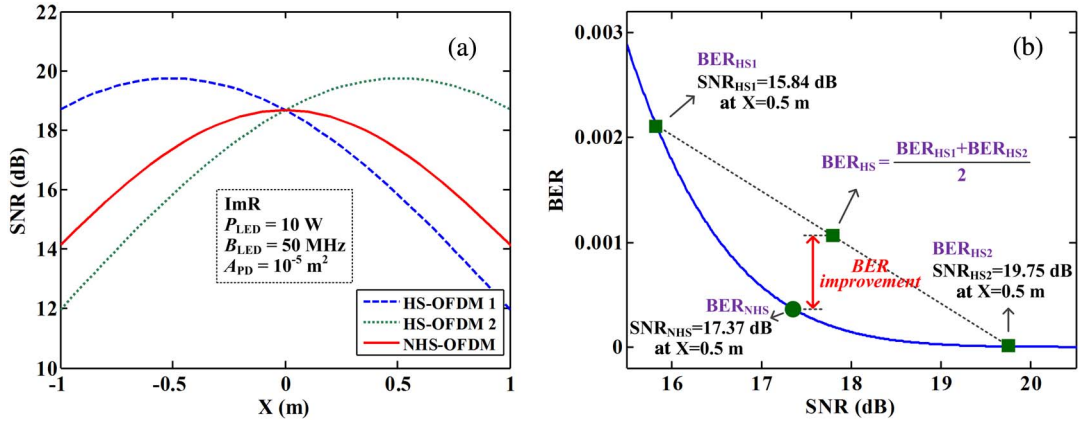

Fig. 3. (a) SNR along the X direction with $Y = 0$ m employing ImR. (b) BER versus SNR for 16QAM-OFDM over an AWGN channel. (P_{LED}, output optical power of LED; B_{LED}, modulation bandwidth of LED; A_{PD}, active area of PD.)

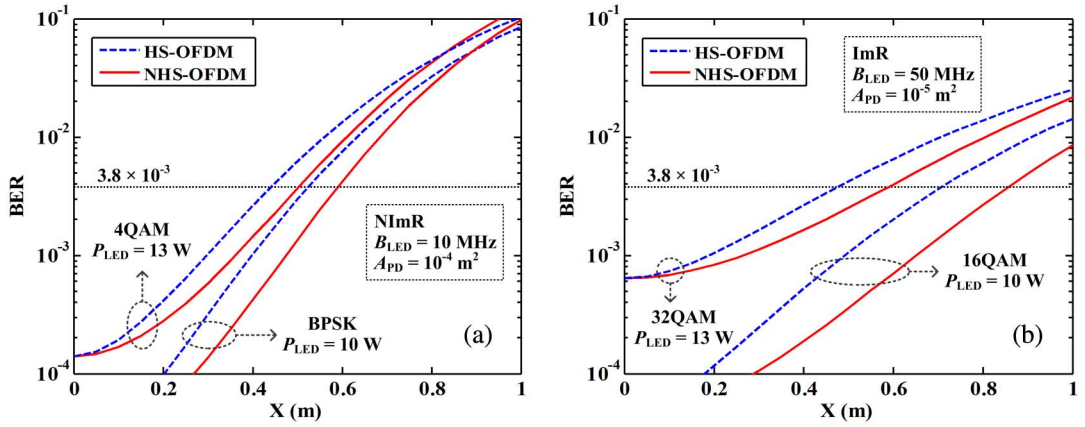

Fig. 4. BER versus receiver position offset along the X direction with $Y = 0$ m for the 2 × 2 MIMO-VLC system employing (a) NImR and (b) ImR. (P_{LED}, output optical power of LED; B_{LED}, modulation bandwidth of LED; A_{PD}, active area of PD.)

MIMO-VLC system employing a NImR and an ImR, respectively. When a NImR is employed, as shown in Fig. 4(a), the modulation bandwidth of LED B_{LED} is set at 10 MHz and the active area of PD A_{PD} is assumed to be 10^{-4} m^2. Due to the high ICI, two lower-order constellations are considered. For a target BER of 3.8×10^{-3}, compared with the system using HS-OFDM, a relative larger receiver position offset can be achieved when using NHS-OFDM, for both binary phase shift keying (BPSK) with an LED output optical power $P_{\mathrm{LED}} = 10$ W and 4QAM with $P_{\mathrm{LED}} = 13$ W. The same conclusion can be drawn for the system employing an ImR, as shown in Fig. 4(b).

Figures 5(a) and 5(b) show the corresponding communication coverage areas of the 2×2 MIMO-VLC system employing a NImR and an ImR, respectively, for a target BER of 3.8×10^{-3}. The coverage contours can be approximated as ellipses, and the coverage areas can be estimated by the areas of ellipses. The area of an ellipse is calculated by $\pi ab/4$, where a and b are the major and minor axes, respectively. As can be seen in Fig. 5(a), for BPSK with $P_{\mathrm{LED}} = 10$ W, two ellipses have the same major axis of 1.7 m; while the minor axes associated with HS-OFDM and NHS-OFDM are 1.04 and 1.2 m, respectively, indicating a coverage improvement of 15.4%. For 4QAM with $P_{\mathrm{LED}} = 13$ W, a coverage improvement of 13.6% is also achieved. Moreover, when an ImR is employed, as shown in Fig. 5(b), the coverage improvements for 16QAM with $P_{\mathrm{LED}} = 10$ W and 32QAM with $P_{\mathrm{LED}} = 13$ W are 21.4% and 20.8%, respectively. The above results show that the coverage improvement is slightly reduced when the order of the constellation is increased.

B. Transceiver Complexity

In an indoor 2×2 MIMO-VLC system using HS-OFDM, as shown in Fig. 1(a), two pairs of HS-OFDM transmitters and receivers are required. However, only one pair of NHS-OFDM transmitter and receiver is required in the system using NHS-OFDM, as shown in Fig. 1(b). Because each HS-OFDM/NHS-OFDM transmitter (receiver) requires one N-point IFFT (FFT) module, the number of the required IFFT and FFT modules in the 2×2 MIMO-VLC system using NHS-OFDM is reduced by half, as compared with the system using HS-OFDM. Note that this conclusion holds for general MIMO-VLC systems with one or multiple pairs of LEDs.

Because the output (input) of the IFFT (FFT) module in HS-OFDM is of real value, the Hermitian symmetric IFFT and real-valued FFT are used. In contrast, complex-valued IFFT and FFT are used in NHS-OFDM. As discussed in [34], the computational complexity of real-valued FFT is largely dependent on the algorithms used. For the algorithm, which treats the real-valued input as a complex-valued input with a zero imaginary part and then applies the complex-valued FFT, the computational complexity of one N-point real-valued FFT is exactly the same as that of one N-point complex-valued FFT [34]. For the algorithm, which exploits the symmetries of real-valued FFT, i.e., the real part of the output is even symmetric, and the imaginary part is odd symmetric, the computational complexity can be reduced by about a factor of 2 [34]. Likewise, the Hermitian symmetric IFFT can be computed by reversing the computation of real-valued FFT [35]. Therefore, depending on the algorithm used for the computation of the Hermitian symmetric IFFT and real-valued FFT, the MIMO-VLC system using NHS-OFDM has lower or nearly the same computational complexity as the system using conventional HS-OFDM.

IV. Experimental Setup and Results

In order to verify the performance of NHS-OFDM in indoor MIMO-VLC systems, a proof-of-concept experimental demonstration using an ImR is performed. The setup of an indoor 2×2 MIMO-VLC system is illustrated in Fig. 6. Two off-the-shelf white LEDs (Luxeon Star) are used as optical transmitters, which have a 3-dB modulation bandwidth of about 2.5 MHz, and the spacing between them is 20 cm. An ImR is configured as the optical receiver, which consists of an imaging lens, two blue filters (BFs), and two PDs

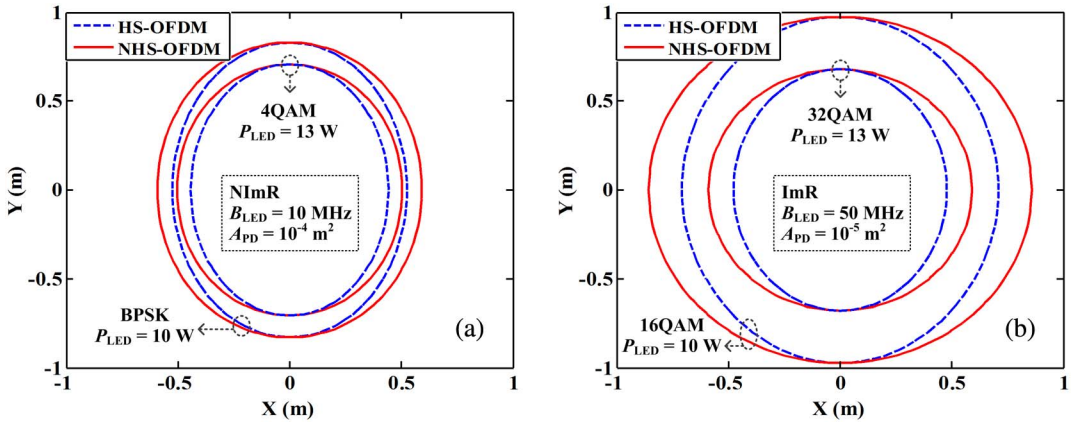

Fig. 5. Communication coverage of the 2×2 MIMO-VLC system for a target BER of 3.8×10^{-3} employing (a) NImR and (b) ImR. (P_{LED}, output optical power of LED; B_{LED}, modulation bandwidth of LED; A_{PD}, active area of PD.)

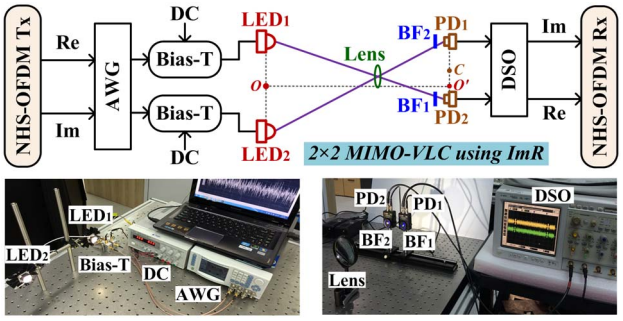

Fig. 6. Experimental setup of the 2 × 2 MIMO-VLC system using ImR.

(Thorlabs, PDA10A, 0.8 mm^2 active area and 180 MHz bandwidth). The imaging lens is placed in front of the two PDs such that each of the two LEDs is precisely imaged onto a corresponding PD. As shown in Fig. 6, O and C are the center points of the two LEDs and the two PDs, respectively, and O' is the foot of the perpendicular from O to the detector plane. Here, we define receiver position offset as the distance between O' and C, and the transmission distance as the distance between O and O'.

The digital NHS-OFDM signal is generated offline by MATLAB with an IFFT size of 256. In order to spectrally separate the baseband signal from high-frequency aliasing products generated by the digital-to-analog converters (DACs), the subcarriers in the high-frequency part are left unmodulated for oversampling, which is also referred to as zero padding [36]. As a result, 128 subcarriers in total are used for data transmission, and no HS is imposed. For fair performance comparison, two independent HS-OFDM signals are also generated with 256-point IFFT. Both oversampling and HS are performed, and 64 subcarriers in total are used for data transmission in each HS-OFDM signal. For both NHS-OFDM and HS-OFDM signals, 16QAM mapping is applied, and the CP length is set to 8, which is 1/32 of the IFFT size. Moreover, a pseudo random binary sequence (PRBS) with the length of 20 is used as the TS for both time synchronization and channel matrix estimation, and 200 OFDM payload symbols are followed for BER measurement. In order to extend the 3-dB modulation bandwidth of the LEDs, digital pre-FDE is performed, and the detailed procedure of pre-FDE can be found in [37].

The Re and Im parts of the complex-valued NHS-OFDM signal are separately loaded into a multichannel arbitrary waveform generator (AWG, Tabor WW2074) with a sampling rate of 200 MSa/s. Therefore, the bandwidth of the Re and Im signals is 50 MHz, and the raw data rate is 400 Mb/s. The analog Re and Im signals are separately superimposed onto 500 mA DC bias currents via two bias-tees (Mini-Circuits, ZFBT-6GW+). The resultant signals are used to modulate the intensities of two LEDs. The luminous flux of each LED is about 63 lm. The light is detected by the ImR, and the received signals are sampled by a digital storage oscilloscope (DSO, Agilent Infiniium 54832B) with a sampling rate of 4 GSa/s. Subsequently, the output digital Re and Im signals are processed offline. For comparison, two HS-OFDM signals

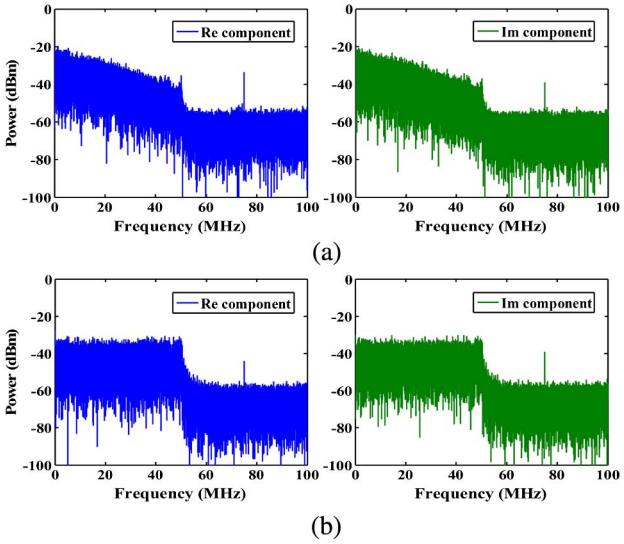

Fig. 7. Measured electrical spectra of the received real (Re) and imaginary (Im) parts of the NHS-OFDM signal (a) without pre-FDE and (b) with pre-FDE.

achieving a total data rate of 400 Mb/s with a bandwidth of 50 MHz are transmitted through the same system.

Figure 7 compares the measured electrical spectra of the received Re and Im parts of the NHS-OFDM signal. Without pre-FDE, as shown in Fig. 7(a), the power of high-frequency components is greatly attenuated, and a power attenuation of about 20 dB is found for both the Re and Im parts. However, the electrical spectra are significantly flattened with a power fluctuation less than 3 dB after performing pre-FDE, as shown in Fig. 7(b).

Figure 8 shows the measured BER performance as a function of the receiver position offset for a transmission distance of 100 cm. As we can see, the BER is always greater than the 7% forward error correction threshold of 3.8×10^{-3} when digital pre-FDE is not performed. However, the BER is substantially reduced after

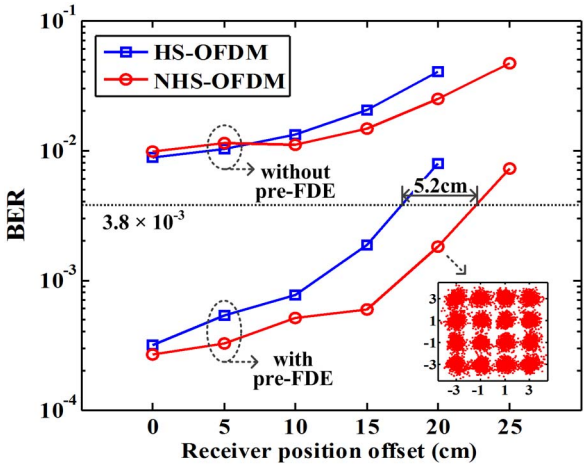

Fig. 8. Measured BER versus receiver position offset with a distance of 100 cm.

performing pre-FDE. It also can be seen that HS-OFDM and NHS-OFDM have nearly the same BER performance when the receiver position offset is 0 cm, and NHS-OFDM outperforms HS-OFDM as the receiver position offset increases. To reach a target BER of 3.8×10^{-3}, the maximum receiver position offsets by using HS-OFDM and NHS-OFDM are 17.4 and 22.6 cm, respectively. Hence, NHS-OFDM achieves a 5.2 cm greater receiver position offset than HS-OFDM. As discussed in Subsection III.A, the communication coverage area of the 2×2 MIMO-VLC system can be approximated as an ellipse, and the coverage areas can be estimated by the areas of ellipses. Two ellipses, associated with HS-OFDM and NHS-OFDM, have the same major axis but a different minor axis. Moreover, the semi-minor axes (half of the minor axes) are given by the corresponding maximum receiver position offsets. Therefore, NHS-OFDM improves the communication coverage of the 2×2 MIMO-VLC system by about 30% for BER $= 3.8 \times 10^{-3}$, compared with HS-OFDM.

V. Conclusion

We have analytically investigated and experimentally demonstrated the proposed NHS-OFDM scheme for an indoor 2×2 MIMO-VLC system. Moreover, the performance of conventional HS-OFDM has also been investigated in such a system for comparison. The analytical results have shown that the 2×2 MIMO-VLC system using NHS-OFDM exhibits computational complexity lower than or comparable to the system using HS-OFDM but achieves superior BER performance. The experimental results have further verified that, for a target BER of 3.8×10^{-3}, NHS-OFDM improves the communication coverage area of a 400 Mb/s imaging 2×2 MIMO-VLC system by about 30% compared with HS-OFDM. In conclusion, NHS-OFDM can be a promising technique for MIMO-VLC-based high-speed indoor wireless access.

Acknowledgment

This work was supported by Ministry of Education-Singapore (MOE)/Nanyang Technological University (NTU) AcRF Tier 1 Grant RG 85/13.

References

[1] T. Komine and M. Nakagawa, "Fundamental analysis for visible-light communication system using LED lights," *IEEE Trans. Consum. Electron.*, vol. 50, no. 1, pp. 100–107, 2004.

[2] Z. Ghassemlooy, W. Popoola, and S. Rajbhandari, *Optical Wireless Communications, System and Channel Modelling With MATLAB*. London: CRC Press, 2012.

[3] H. Haas, "Visible light communication," in *Optical Fiber Communication Conf. (OFC)*, Los Angeles, CA, Mar. 22–26, 2015, paper Tu2G.5.

[4] H. Elgala, R. Mesleh, and H. Haas, "Indoor optical wireless communication: Potential and state-of-the-art," *IEEE Commun. Mag.*, vol. 49, no. 9, pp. 56–62, 2011.

[5] H. Le-Minh, D. O'Brien, G. Faulkner, L. Zeng, K. Lee, D. Jung, and Y. Oh, "High-speed visible light communications using multiple-resonant equalization," *IEEE Photon. Technol. Lett.*, vol. 20, no. 14, pp. 1243–1245, 2008.

[6] Y. F. Liu, Y. C. Chang, C. W. Chow, and C. H. Yeh, "Equalization and pre-distorted schemes for increasing data rate in indoor visible light communication system," in *Optical Fiber Communication Conf. (OFC)*, 2011, paper JWA083.

[7] L. Zeng, D. O'Brien, H. Minh, G. Faulkner, K. Lee, D. Jung, Y. Oh, and E. Won, "High data rate multiple input multiple output (MIMO) optical wireless communications using white LED lighting," *IEEE J. Sel. Areas Commun.*, vol. 27, no. 9, pp. 1654–1662, 2009.

[8] T. Fath and H. Haas, "Performance comparison of MIMO techniques for optical wireless communication in indoor environments," *IEEE Trans. Commun.*, vol. 61, no. 2, pp. 733–742, 2013.

[9] N. Ishikawa and S. Sugiura, "Maximizing constrained capacity of power-imbalanced optical wireless MIMO communications using spatial modulation," *J. Lightwave Technol.*, vol. 33, no. 2, pp. 519–527, 2015.

[10] Y. Wang, N. Chi, Y. Wang, R. Li, X. Huang, C. Yang, and Z. Zhang, "High-speed quasi-balanced detection OFDM in visible light communication," *Opt. Express*, vol. 21, no. 23, pp. 27558–27564, 2013.

[11] C. Yeh, H. Chen, C. Chow, and Y. Liu, "Utilization of multiband OFDM modulation to increase traffic rate of phosphor-LED wireless VLC," *Opt. Express*, vol. 23, no. 2, pp. 1133–1138, 2015.

[12] L. Wu, Z. Zhang, J. Dang, and H. Liu, "Adaptive modulation schemes for visible light communications," *J. Lightwave Technol.*, vol. 33, no. 1, pp. 117–125, 2015.

[13] A. H. Azhar, T.-A. Tran, and D. O'Brien, "A gigabit/s indoor wireless transmission using MIMO-OFDM visible-light communications," *IEEE Photon. Technol. Lett.*, vol. 25, no. 2, pp. 171–174, 2013.

[14] S. D. Dissanayake and J. Armstrong, "Comparison of ACO-OFDM, DCO-OFDM, and ADO-OFDM in IM/DD systems," *J. Lightwave Technol.*, vol. 31, no. 7, pp. 1063–1072, 2013.

[15] D. Tsonev, S. Sinanovic, and H. Haas, "Novel unipolar orthogonal frequency division multiplexing (U-OFDM) for optical wireless," in *Proc. IEEE Vehicular Technology Conf. (VTC Spring)*, 2012, pp. 1–5.

[16] D. Tsonev and H. Haas, "Avoiding spectral efficiency loss in unipolar OFDM for optical wireless communication," in *Proc. IEEE Int. Conf. Communication (ICC)*, 2014, pp. 3336–3341.

[17] H. Elgala and T. D. C. Little, "SEE-OFDM: Spectral and energy efficient OFDM for optical IM/DD systems," in *Proc. IEEE Int. Symp. Personal, Indoor and Mobile Radio Communications (PIMRC)*, 2013, pp. 486–490.

[18] N. Wu and Y. Bar-Ness, "A novel power-efficient scheme asymmetrically and symmetrically clipping optical (ASCO)-OFDM for IM/DD optical systems," *EURASIP J. Adv. Signal Process.*, vol. 3, article 3, 2015.

[19] M. S. Moreolo, R. Muñoz, and G. Junyent, "Novel power efficient optical OFDM based on Hartley transform for intensity-modulated direct-detection systems," *J. Lightwave Technol.*, vol. 28, no. 5, pp. 798–805, 2010.

[20] H. Elgala and T. Little, "P-OFDM: Spectrally efficient unipolar OFDM," in *Optical Fiber Communication Conf. (OFC)*, 2014, paper Th3G.7.

[21] H. Elgala and T. Little, "Polar-based OFDM and SC-FDE links towards energy-efficient Gbps transmission under

IM-DD optical system constraints," *J. Opt. Commun. Netw.*, vol. 7, no. 2, pp. A277–A284, 2015.

[22] F. Barrami, Y. Guennec, E. Novakov, J.-M. Duchamp, and P. Busson, "A novel FFT/IFFT size efficient technique to generate real time optical OFDM signals compatible with IM/DD systems," in *Proc. European Microwave Conf. (EuMC)*, 2013, pp. 1247–1250.

[23] A. Nuwanpriya, A. Grant, S.-W. Ho, and L. Luo, "Position modulating OFDM for optical wireless communications," in *Proc. IEEE Global Communication Conf. (GLOBECOM)*, 2012, pp. 1219–1223.

[24] M. Z. Afgani, H. Haas, H. Elgala, and D. Knipp, "Visible light communication using OFDM," in *Proc. Int. Conf. Testbeds Research Infrastructures Development Networks Communities (TRIDENTCOM)*, 2006, pp. 129–134.

[25] Y. Chen, C. Yang, Q. Yang, W. Liu, C. Li, and D. Zhang, "Wavelet transform-OFDM in indoor visible light communication," in *Optical Fiber Communication Conf. (OFC)*, 2015, paper W2A.62.

[26] P. Butala, H. Elgala, and T. Little, "Performance of optical spatial modulation and spatial multiplexing with imaging receiver," in *Proc. IEEE Wireless Communication Networking Conf. (WCNC)*, 2014, pp. 394–399.

[27] T. Chen, L. Liu, B. Tu, Z. Zheng, and W. Hu, "High-spatial-diversity imaging receiver using fisheye lens for indoor MIMO VLCs," *IEEE Photon. Technol. Lett.*, vol. 26, no. 22, pp. 2260–2263, 2014.

[28] T. Chen, Z. Zheng, L. Liu, and W. Hu, "High-diversity space division multiplexing visible light communication utilizing a fisheye-lens-based imaging receiver," in *Optical Fiber Communication Conf. (OFC)*, 2015, paper Tu2G.3.

[29] C. Chen, W.-D. Zhong, and D. Wu, "Communication coverage improvement of indoor SDM-VLC system using NHS-OFDM with a modified imaging receiver," in *Proc. IEEE Int. Conf. Communication (ICC) Workshops*, 2016, pp. 315–320.

[30] Z. Wang, C. Yu, W.-D. Zhong, and J. Chen, "Performance improvement by tilting receiver plane in M-QAM OFDM visible light communications," *Opt. Express*, vol. 19, no. 14, pp. 13418–13427, 2011.

[31] H. Burchardt, N. Serafimovski, D. Tsonev, S. Videv, and H. Haas, "VLC: Beyond point-to-point communication," *IEEE Commun. Mag.*, vol. 52, no. 7, pp. 98–105, 2014.

[32] A. Burton, H. Minh, Z. Ghassemlooy, E. Bentley, and C. Botella, "Experimental demonstration of 50-Mb/s visible light communications using 4×4 MIMO," *IEEE Photon. Technol. Lett.*, vol. 26, no. 9, pp. 945–948, 2014.

[33] K. Cho and D. Yoon, "On the general BER expression of one- and two-dimensional amplitude modulations," *IEEE Trans. Commun.*, vol. 50, no. 7, pp. 1074–1080, 2002.

[34] H. Sorensen, D. Jones, M. Heideman, and C. Burrus, "Real-valued fast Fourier transform algorithms," *IEEE Trans. Acoust., Speech, Signal Process.*, vol. 35, no. 6, pp. 849–863, 1987.

[35] H.-F. Chi and Z.-H. Lai, "A cost-effective memory-based real-valued FFT and Hermitian symmetric IFFT processor for DMT-based wire-line transmission systems," in *Proc. IEEE Int. Symp. Circuits and Systems (ISCAS)*, 2005, pp. 6006–6009.

[36] X. Li, W.-D. Zhong, A. Alphones, C. Yu, and Q. Yang, "Channel equalization based on QR decomposition in indoor visible light communication," in *Proc. IEEE Conf. Industrial Electronics Applications (ICIEA)*, 2015, pp. 1491–1495.

[37] J. Li, Z. Huang, X. Liu, and Y. Ji, "Hybrid time-frequency domain equalization for LED nonlinearity mitigation in OFDM-based VLC systems," *Opt. Express*, vol. 23, no. 1, pp. 611–619, 2015.